Chapter 9

Induction Linac

9.1 Induction Accelerators for the Phase Rotator System

The principle of magnetic induction has often been applied to the acceleration of high-current beams in betatrons and in a variety of induction accelerators [1]. The induction linac (IL) consists of a simple nonresonant structure where the drive voltage is applied to an axially symmetric gap that encloses a toroidal ferromagnetic material. The change in flux in the magnetic core induces an axial electric field that provides particle acceleration. This simple nonresonant (low-Q) structure acts as a single-turn transformer that can accelerate beams of hundreds of amperes to tens of kiloamperes, limited only by the drive impedance. The IL is typically a low-gradient structure that can provide acceleration fields of varying shapes and time durations from tens of nanoseconds to several microseconds. The efficiency of the IL depends on the beam current, and can exceed 50% if the beam current exceeds the magnetization current required by the ferromagnetic material. The acceleration voltage available is simply given by the expression $V = AdB/dt$. Hence, for a given cross sectional area A of material, the beam pulse duration influences the energy gain. Furthermore, there is a premium put on minimizing the core diameter, as this impacts the total weight, or cost, of the magnetic material. Indeed, the diameter doubly impacts the cost of the IL, since the power to drive the cores is proportional to the volume as well.

To meet the waveform requirements during the beam pulse, we make provisions in the pulsing system to maintain the desired $\frac{dB}{dt}$ during the useful part of the acceleration cycle. This can be done in either of two ways: by using the final stage of the pulse forming network (PFN) or by using the pulse-compensation network in close proximity

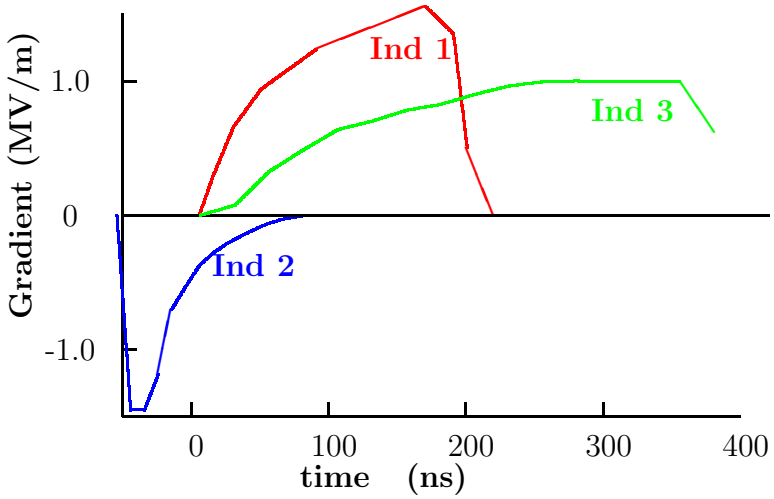

Figure 9.1: Acceleration waveforms for induction 1, 2 and 3.

to the acceleration cell.

The choice of magnetic materials is made by testing various materials, both ferromagnetic and ferrimagnetic; not only to determine the properties that are essential in this application, possible materials will include the nickel-iron, silicon steel, amorphous, and various types of ferrites, but on the energy losses in the magnetization process, which directly impact the cost.

9.1.1 Accelerator Waveforms

Parameters and pulse shapes from this study, compared with Study-I [2] have evolved toward considerably improved physics performance and less demanding accelerator waveforms, avoiding the need for multipulsing.

The present baseline design results in the acceleration waveforms shown in Fig. 9.1. The waveforms for IL1, IL2, and IL3 are all unipolar.

Although IL1 and IL3 could possibly be combined, it became preferable for technical reasons, and to reduce the risk factors, to separate the two functions (with a small penalty in economics). (A combined IL2 and IL3 would require the application of *branched magnetics* to achieve two waveforms that are independently controllable in shape and timing. The branched magnetics approach could lead to a 5-10% cost savings, but at more risk, since this approach has only been applied to small benchtop prototypes but

not to presently operating induction accelerators. This approach will be examined in Appendix B.)

9.1.2 Magnetic Material

A number of induction linac have been constructed in the past that cover the pulse duration of the three units required by the Neutrino Factory. None of these accelerators, however, has gradients and energy gains that are as high. To satisfy the requirements in an economically reasonable design, it is imperative to choose a magnetic material, and a pulsing system, that minimize the cost but still achieve the reliability and performance required.

In the past two decades, great strides have been made in the development of a magnetic material that is replacing all previous ones in the 60-Hz power industry because of its low loss, ease of manufacturing, and low cost. Several alloys are made in ribbon form by rapidly quenching a stream of molten material on a cold rotating drum. The ribbon thickness is typically 25 μm and can be of any width from 5 to 20 cm. Because the ribbon is so thin, and has higher resistivity than other ferromagnetic materials, it is directly applicable to short pulse applications. In short pulse applications where the rate of magnetization (dB/dt) is very high, tens of volts are generated between the layers of ribbon when it is wound into a toroid. Thin insulation such as 2-4 μm Mylar must be used between layers to insure that the ribbon layers are sufficiently insulated to hold off the voltage generated.

The soft magnetic properties can be improved by annealing. Unfortunately, this procedure, although well below the crystallization temperature, embrittles the material, making it nearly impossible to wind into a toroid. Annealing can be done after winding if the insulating material between layers has a sufficiently high melting point. Annealing is not an option when Mylar is used. Coatings have been developed that allow annealing after winding, but at the present time they are not fully developed and do not hold off sufficient voltage per turn. Because the losses at high magnetization rates are almost entirely due to the eddy current losses, very little is lost in our application using the material "as cast" or unannealed.

To choose the appropriate alloy of this amorphous material it is important to measure the properties such as flux swing (ΔB) and magnetization (ΔH) at the appropriate pulse duration or magnetization rate (dB/dt). Figure 9.2 shows the losses in J/m^3, at different rates of magnetization. It can be seen that above T/μs the losses increase linearly with magnetization rate. From Fig. 9.2 it appears that the lowest loss material is the alloy 2705M with the lowest ΔB of about 1.4 T while the highest loss material is 2605CO

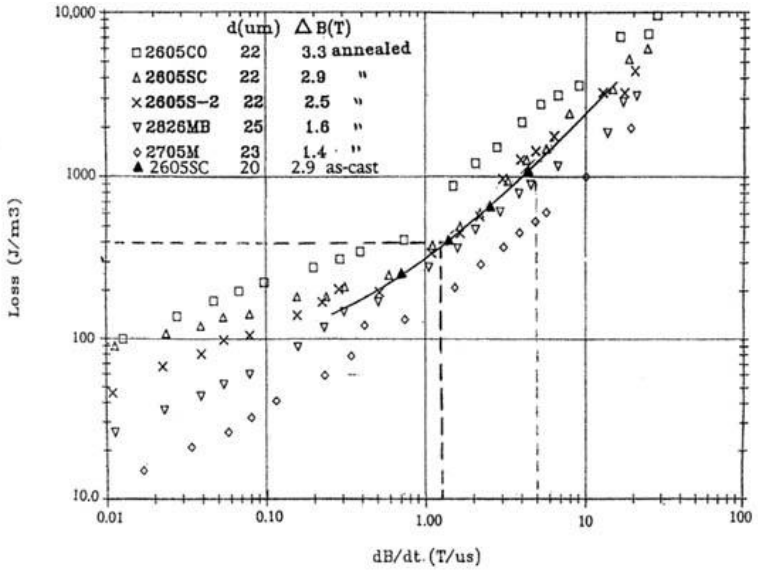

Figure 9.2: Losses (J/m^3) of several amorphous alloys as a function of magnetization rate (dB/dt).

with a ΔB of about 3.3 T. The optimum material is selected by considering the ΔB, the losses (J/m^3) and the cost per kilogram. Two alloys which are not plotted on this chart (Fig. 9.2) are the 2605SA1, used exclusively in the 60-Hz power industry, and the 2605S3A, which is used in pulse transformer applications. The SA1 material offers the potential for greatest savings since it is mass produced for the power industry, but it has not been investigated as thoroughly as the SC or S3A materials at the very short pulse regime of interest here. For this reason the SC alloy is chosen here since it has been used recently in an induction accelerator for radiography at the Los Alamos National Laboratory and extensive technical and cost data exist. The S3A also offers a good choice since it has been used extensively in the AVLIS program at the Lawrence Livermore National Laboratory. The SA1 alloy will be investigated in the near future as part of our R & D program since, as mentioned previously, it offers the greatest possibility for cost savings.

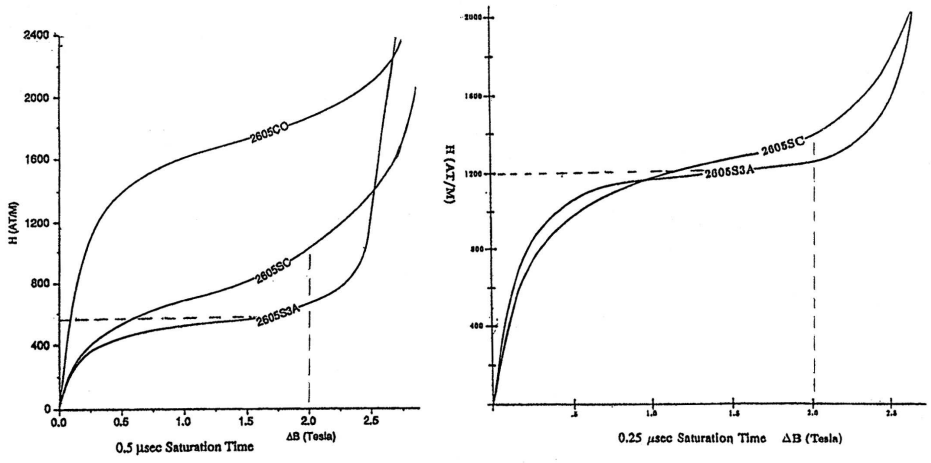

Figure 9.3: Hysteresis for 2605SC and 2605S3A at two different magnetization rates.

9.1.3 Induction Linac 1 Cell

From the specifications 1 in this Study, IL1 is 100 m in length and has the acceleration waveform shown in Fig. 9.1. The waveform has a full-width-half-maximum (FWHM) of about 180 ns, with an approximately exponential rise time of 100 ns and a fast fall time. The significant portion of the acceleration cycle is during the rise time; the fall time is unimportant. In fact, the fall time will be longer than indicated by the waveform since the energy stored in the cell inductance will decay with a time constant $t = L/R$ of the drive circuit. The L/R of the fall time will be similar to the rise time, hence, the actual FWHM will be about 250 ns. Since a 1-m section must allow axial space for the cryogenic feed lines and for vacuum pumping, the maximum allowable space for the core is 712 mm. To obtain the lowest cost for the amorphous material, the alloy should be cast in widths of 101.6 mm (4") or greater. Manufacturing limits, therefore, dictate a maximum number of cells that is a multiple of 101.6 mm. For our case, we select 7 cells.

From the required gradient we now have a basis for calculating the cross-sectional area of the magnetic material for IL1. From $V = A(dB/dt)(\mathrm{PF})$ we can calculate the ΔR knowing the ΔZ and the packing factor (PF=0.75). The hysteresis loop for the two alloys, 2605SC and 2605S3A, are shown in Fig. 9.3.

Although the total flux swing to saturation is over 2.5 T, the actual working flux swing (ΔB) is chosen as 2.0 T so that the pulse generator drives into a more linear load.

The required voltage for each of the seven cells that constitute one meter of acceleration is 214.3 kV. The actual cross-section is

$$A = (r_2 - r_1) * w = \frac{V\Delta t}{\Delta B(PF)} \tag{9.1}$$

so

$$(r_2 - r_1) = frac(214.3 \times 10^3)(250 \times 10^{-9})(2.0)(0.75)(r_2 - r_1) = 0.325 \text{ m}. \tag{9.2}$$

The inside radius of the core is set by the outside radius of the superconducting solenoid at a minimum of 0.4 m. Preliminary calculations of the leakage flux at the solenoid gaps indicate that this flux, which is orthogonal to the magnetization flux, can be of the order of a few thousand gauss at the 0.4 m radius. From previous tests for the Advanced Test Accelerator (ATA) and the Dual-Axis Radiographic Hydro Test (DARHT) [3] accelerator, this is acceptable. Nonetheless, this issue should be investigated further with laboratory tests to insure that the flux swing of the induction cell is not reduced by this stray flux. To be conservative, we set the inside radius of the actual amorphous material at 500 mm. The magnetizing current and the losses can now be calculated. The magnetizing force $\Delta H = \Delta I/\pi d$ where d is the average diameter or $d = r_2 + r_1 = 1.35$ m. From Fig. 9.3 for a 0.25 μs saturation time we find that the magnetizing force is $\Delta H = 1200$ A/m or $\Delta I = 5{,}087$ A, and the loss is $U = V\ \Delta I\ \Delta t$ or $U = (214.3 \times 10^3)(5.087 \times 10^3)(250 \times 10^{-9}) = 272.5$ J/cell. The magnetic material volume, including the mylar insulation is $V = \pi(r_2^2 - r_1^2)(\Delta z)$, or V=0.151 m^3. With a packing factor of 0.75, the actual volume of amorphous material is 0.113 m^3, and at a density of 7290 kg/m^3 it weighs 825 kg. The core losses could also have been calculated from Fig. 9.2, which shows that the losses per cubic meter at a magnetization rate $dB/dt = 2.0$ T/0.25 μs, are 2 kJ/m^3 for a total of 262 J, slightly lower than the estimate above. The loss calculations above determine the drive power required by the pulse generator for one cell. For seven cells $P = 7VI$, and with $V = 214.3$ kV, $I = 5.09$ kA, $P = 7.63$ GW and the impedance $Z = V/7I = 6.0\Omega$.

9.1.3.1 High Voltage Design of Cell

Figure 5.8 shows a cross section of the induction cell. The cell is driven by two high voltage cables at 180°. The high voltage cables plug into two connections, of the type used on the DARHT accelerator, that are part of the compensation network box. The acceleration gap is 1 cm and is oil filled. From Fig. 9.5, which shows the voltage breakdown in oil for different pulse durations and surface areas, it appears that the safety factors are more than adequate, that is, the actual breakdown is about twice the operating voltage. The highest voltage stress occurs at the outside radius of the core where one half of the driving

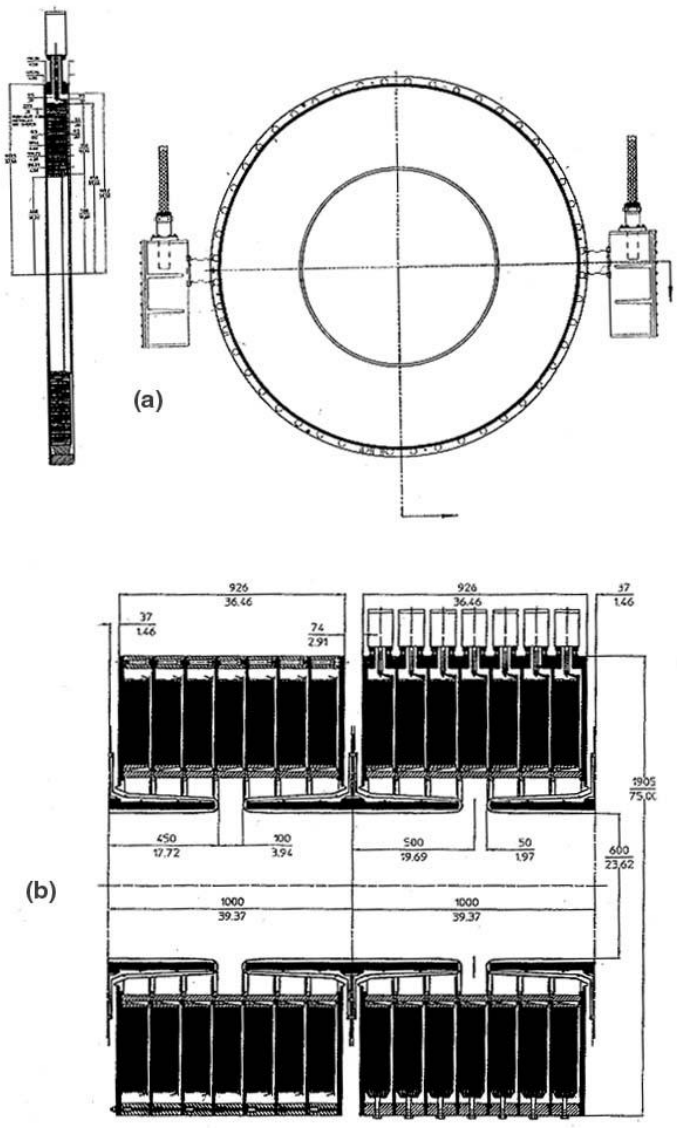

Figure 9.4: (a) Cross section of a single cell with compensation network boxes; (b) cross section of a 2 m section.

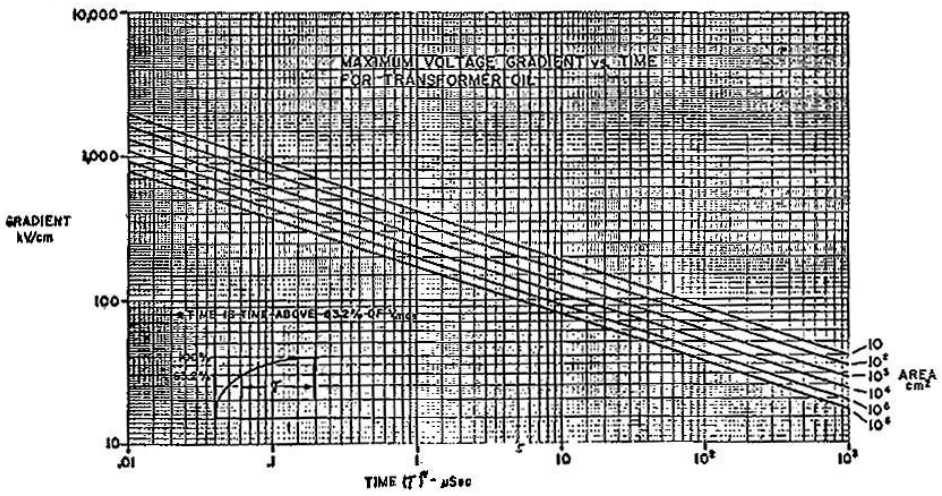

Figure 9.5: Short-pulse voltage breakdown in oil.

voltage appears from each side of the core to ground. Insulation is done with ten layers of 50 μm mylar with oil impregnation.

The oil-to-vacuum interface insulator is designed so that on the vacuum side the field lines form a 30° or greater angle with the insulator to achieve the highest possible voltage holding. The empirical curve in Fig. 9.6 shows the voltage flashover for different angles. For our design, the maximum surface gradient on the insulator is nearly one order of magnitude lower.

The highest voltage gradient occurs between the solenoid housings. Here the spacing is 100 mm and the radius is 30 mm. Using a cylindrical geometry, the maximum gradient is about 150–200 kV/cm. Figure 9.7 shows field emission after 200 ns for different types of surfaces. A standard electropolished stainless steel surface is marginally acceptable for our purposes. To be prudent, the surfaces should be greened. In a subsequent optimization, the gradient will be reduced somewhat by redesigning the nose pieces.

9.1.4 Induction Linac 2 Cell

From the specifications shown in Fig. 9.1 for IL2, the deceleration pulse has an unspecified rise time (from zero to a negative value) and a fall time of about 50 ns (from a negative

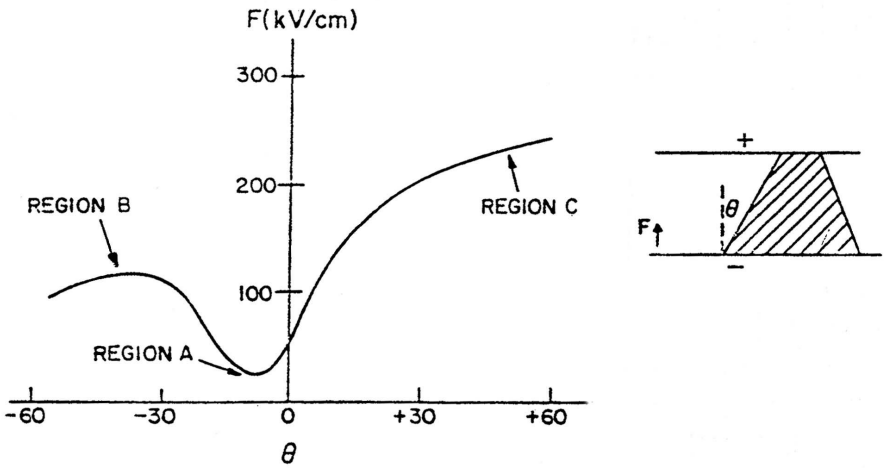

Figure 9.6: Flashover voltage with a 30-ns pulse for different cone angles.

value back to zero) that is a significant portion of the waveform.

Induction accelerators with pulse durations of less than 100 ns have traditionally used nickel-zinc ferrites as the magnetic material of choice. This choice was the appropriate one a decade or two ago when the last short-pulse induction accelerator was built, since the amorphous materials at that time were not of a very high quality and were more expensive than they are today. The choice of ferrites also was logical if one compares their losses to those of amorphous materials at saturation times of 50 ns. We can see from Fig. 9.8 that, if full saturation is achieved in 50 ns, the losses for ferrites (CMD 5005) are about 800 J/m^3 while the losses for amorphous materials (2605SC) are about one order of magnitude higher. That is, even though the flux swing for amorphous materials is five times greater than those of the ferrites, the losses are more than ten times greater (at full saturation). On the other hand, the cost of ferrites has quadrupled in the past two decades while the cost of amorphous materials has decreased considerably. This makes it imperative to take another look at using amorphous materials of the same cross section (volume) as the ferrites. Then the flux swing would be much lower than that at full saturation, as would be the magnetization rates, and hence, the losses. To make the best comparison, designs were made using both the ferrites and the amorphous materials. Using the standard 101.6 mm width (w) and a ΔB (from Fig. 9.9) for the ferrite CMD-5005 the area $A = w(r_2 - r_1) = V\Delta t/\Delta B$. From Fig. 9.1 the significant part of the

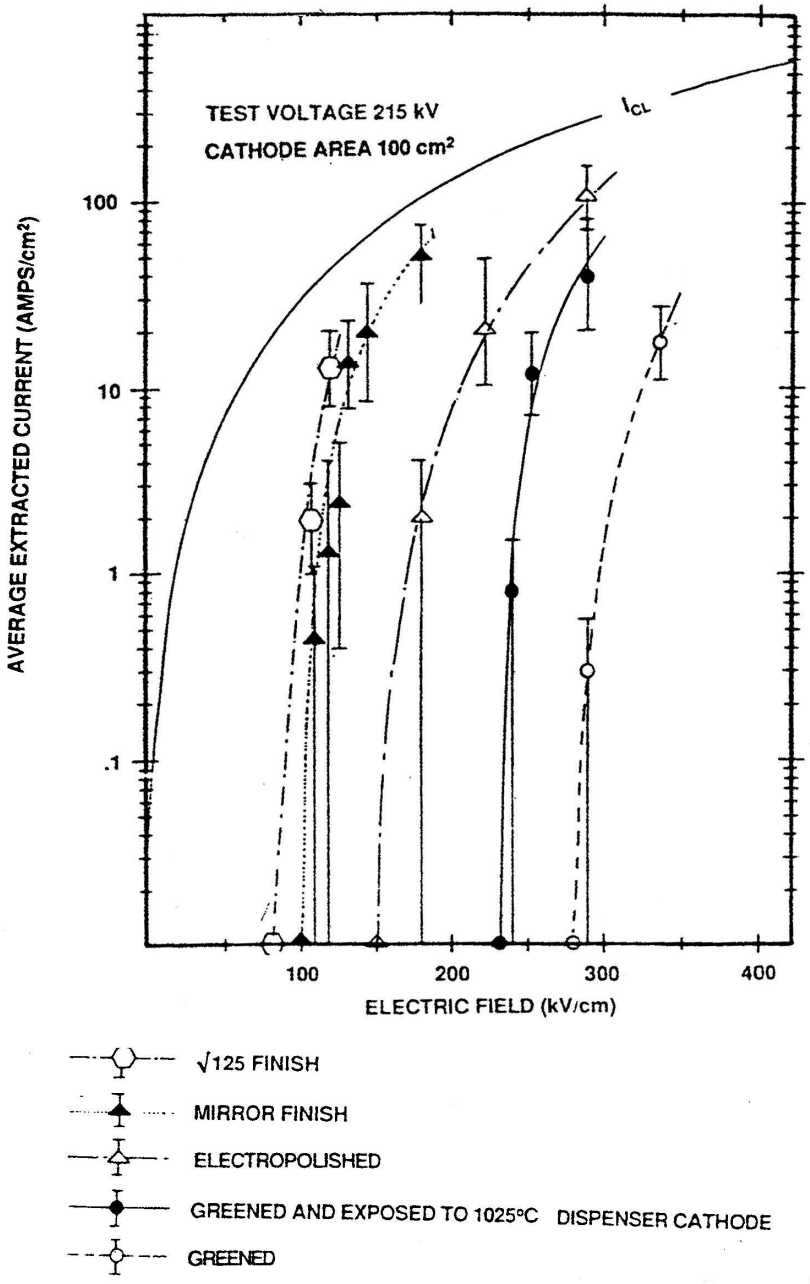

Figure 9.7: Current density after 200 ns for different surface preparations.

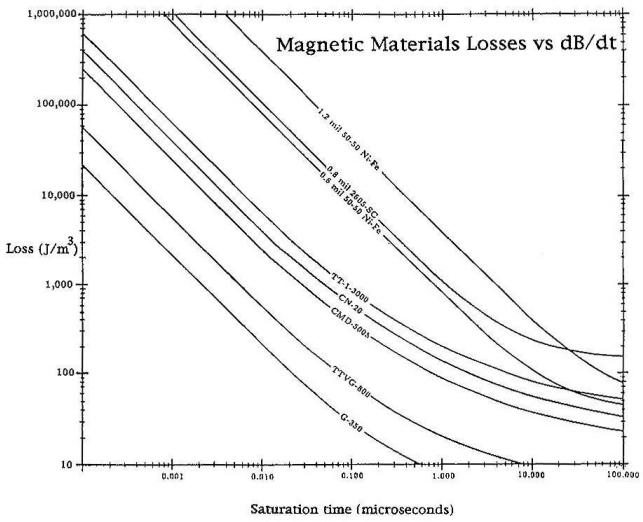

Figure 9.8: Magnetic material losses for different saturation times.

acceleration waveform is the fall time while the rise time is unspecified and is determined by the pulse generators. Because of the large gap capacitance and the impedance of the pulse generator, the rise time will be nearly the same as the fall time so that the FWHM will be about 100 ns.

Using 100 ns as Δt and the voltage per cell V = 188 kV, the outside radius r_2 = 870 mm. From Fig. 9.9, the hysteresis curve for CMD-5005 indicates that ΔH = 1000 A/m and the losses will be 500 J/m^3. The ferrite volume, $V = \pi(r_2^2 - r_1^2)$ = 0.162 m^3 will result in 81 J of losses per cell requiring a drive current I = 4.3 kA. Taking the same cross-sectional area, but using the properties of amorphous materials, we can compare the losses. Because the packing factor of the amorphous material will be 0.75 instead of 1, the flux swing will be 0.667 T and the magnetization rate dB/dt = 6.67 T/μs (for, 100 ns saturation). From Fig. 9.2, the losses for 2605SC are about 1400 J/m^3. The total losses, U, for the amorphous material will be U = (1400 J/m^3)(0.162 m^3)(0.75) or U = 170 J/cell. We conclude that losses using the amorphous material are about twice as high as those of the ferrites and, therefore, the cost of the pulse generator will be that much greater. Surprisingly, the economics still favor the amorphous material because its cost is about one-fourth of that of the ferrites. Even though the pulse generator doubles in cost, the net result is a saving of about 10%.

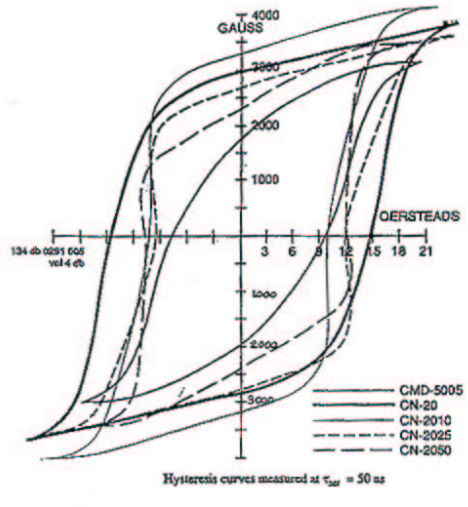

Figure 9.9: Hysteresis curves for various ferrites.

It is interesting to note that the design for IL2 is nearly identical to IL1, that is, $r_2 = 0.85$ m for IL1 and $r_2 = 0.87$ m for IL2, so in actuality, for manufacturing and design cost saving, the two cells can be identical. Since IL2 is a decelerating gradient, the induction cells for this accelerator are simply installed rotated 180° from those of Induction 1.

9.1.5 Induction Linac 3 Cell

Applying the same arguments used in the design of IL1, the FWHM for IL3 is 380 ns and the acceleration voltage $V = 143$ kV. The outside radius of this cell can now be calculated from $V\ \Delta t = A\Delta B(\text{PF})$. The magnetization rate for this cell is lower since the saturation time is longer. For the same ΔB as in IL1, or $\Delta B = 2.0$ T, $dB/dt = 5.26$ T/μs, and the magnetization will be the average between the two cases shown in Fig. 9.3 or $\Delta H = 900$ A/m. Applying these parameters to the design of IL3, from $w(r_2 - r_1) = \frac{V\Delta t}{\Delta B(PF)}$ we get $r_2 = 857$ mm. The magnetizing current is $I = \pi H(r_2 + r_1) = 3.84$ kA and the cell losses $U = VI\Delta t = (143 \times 10^3)(3.84 \times 10^3)(380 \times 10^{-9}) = 209$ J. The volume of material is $V = \pi(r_2^2 - r_1^2)w = 0.155$ m^3, and the weight with a PF = 0.75, is 846 kg. Table 9.1 summarizes important parameters for the three induction accelerators.

It is evident from Table 9.1 that the three induction accelerators can be mechanically identical as far as induction cells are concerned. Each pulsing system will, of course, be

Table 9.1: Induction accelerator parameters.

Unit	MV/m	Length (m)	Δt (ns)	IR (m)	OR (m)	V_{cell} (m^3)	W_{cell} (kg)	ΔB (T)	ΔH (A/m)	Voltage (kV)	Current (kA)	Energy (J)	Weight (tons)
IL1	1.5	100	250	0.5	0.85	0.151	826	2.0	1200	214	5.09	273	578
IL2	1.5	80	100	0.5	0.87	0.162	886	0.67	2100	188	9.05	170	496
IL3	1.0	80	380	0.5	0.86	0.155	846	2.0	900	143	3.84	209	474

different.

The amorphous alloy taken for this Study was not optimized but was chosen because the most reliable information exists for it in the short-pulse applications and the most accurate cost data was available from a recent induction linac constructed at LANL for radiography. It is very likely that the alloy being mass produced for the power industry, 2605SA1, can be substituted for the 2605SC. The SA1 material has great potential for cost reduction, since it is mass produced in very large quantities. We will pursue testing samples of SA1 in the near future as part of the R&D program, and will begin negotiations with the scientific staff at Honeywell (Allied Signal) to explore making the material in thinner ribbon and less expensive than the SC material.

9.1.6 Pulsing System

IL1, IL2, and IL3 are driven by pulse generators with output voltages from 100–200 kV and currents in the tens of kiloamperes at pulse durations from 50 ns to 300 ns. The peak power levels exceed 1 GW and, except for spark gaps, no switches exist that are capable of operating reliably at the required repetition rates and power levels. The prefered option, then, is the nonlinear magnetic pulse compression modulator.

The use of saturable reactors for generating very high peak power levels was described by Melville [4] in 1951. The basic principle behind magnetic pulse switching [5] is to use the large changes in permeability exhibited by saturating ferri-(ferro) magnetic materials to produce large changes in impedance. The standard technique for capitalizing on this behavior is shown on Fig. 9.10. By using multiple stages, as shown, it is possible to compress a pulse of relatively low power and long duration into a pulse of very high peak power and very short duration, maintaining the same energy (except for a small core loss) per pulse. This is exactly the technique that allows us to use available thyratrons or solid-state devices to initiate the pulse and then pulse compress it to the desired peak power levels.

The principle of operation of the magnetic pulse compressor has been covered extensively in the literature but is briefly described here for completeness. Referring to Figure

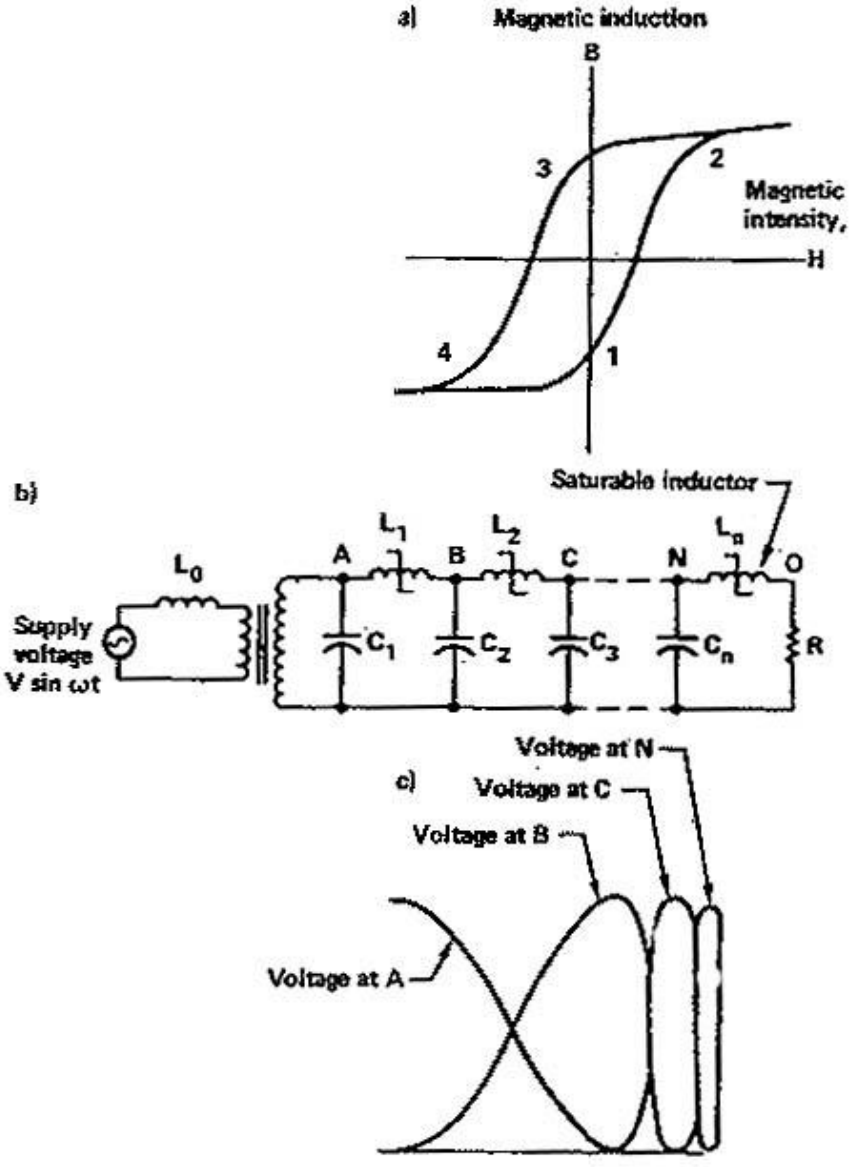

Figure 9.10: Principle of magnetic pulse compression.

5.14, capacitor C_1 charges through inductance L_0 until inductance L_1 saturates, becoming much less than L_0. Once this happens, C_2 will begin to charge from C_1 through L_{1sat} but since L_{1sat} is much less than L_0, C_2 charges more rapidly than C_1 did. This process continues through the successive stages until C_n discharges into the load through L_{nsat}.

To make this process efficient, we design each of these successive stages so that saturation occurs at the peak of the voltage waveform. Segment 1 to 2 in the hysteresis loop of Fig. 9.10 is the active, or high-permeability, region during which the inductor impedes current flow; the leveling off of the curve at point 2, reached at the peak of the voltage waveform, indicates core saturation when the inductor achieves a low impedance. During segment 2 to 4, the core is reset to its original state, ready for the next cycle.

9.1.6.1 IL1 pulse compressor

The requirement for IL1 is to generate an acceleration pulse shape and gradient shown in Fig. 4.5. Each accelerator cell previously described produces a voltage of 214 kV; after the beam traverses 700 of these cells it has gained 150 MV of energy. From Table 9.1, the necessary drive current for one cell is 5.09 kA for a duration (FWHM) of 250 ns. As previously mentioned, no switches exist that can produce this type of pulse directly. By investigating the optimum operating voltage and current of the switches, the required stages of compression are decided. Since thyristors have limits in dI/dt of several kA/μs and voltage limits of a few kV it can be seen that a large number of them in series and parallel combination will be required. Thyratrons also have limits on dI/dt and voltage but these limits are at least one order of magnitude greater than thyristors. Thyristors have practically unlimited life while thyratrons have an operating life of the order of 20,000 hours. Even taking into consideration replacement costs, the thyratrons offer a simpler and more economical pulse compression system (fewer stages).

For technical and economic reasons, the pulse compression system is designed to drive one meter or seven induction cells. The total energy required is $U = 273 \times 7 = 1.9$ kJ plus that needed to make up the additional losses incurred in the pulse compression scheme. The 500 J pulse compression system (Fig. 9.12), designed to replace the Advanced Test Accelerator spark gaps, achieved efficiencies greater than 90%. Allowing for 5% losses in the thyratron switches, 5% losses in the resonant charging and 5% in the power supply, the total input energy per pulse needed is 2.5 kJ and, at 15 Hz average repetition rate, the power for seven cells $P = 38.2$ kW; the total power for IL1 is $P_t = 3.82$ MW.

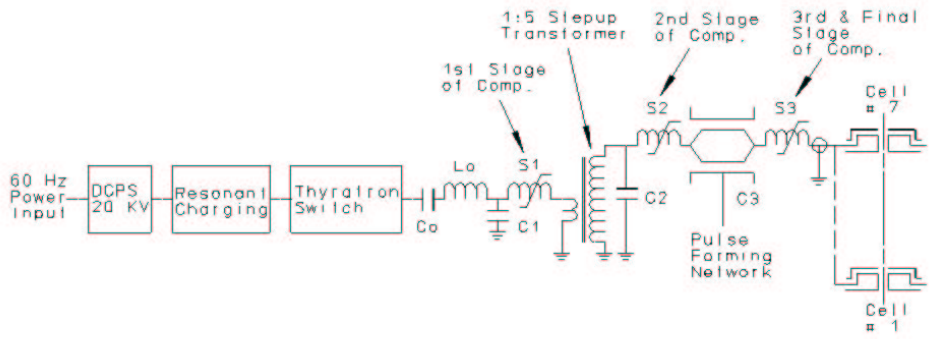

Figure 9.11: Simplified diagram of IL1 7-cell pulse generator.

9.1.6.2 IL1 7-Cell pulse generator

Figure 9.11 shows a simplified diagram of the pulse generator that will drive 7 cells of IL1 with a voltage pulse of 214 kV, 35.6 kA and a pulse duration FWHM = 250 ns. The resonant charger initiates the sequence by charging capacitor C_0 to $2 \times V_{DCPS}$ or 30–40 kV. The charging current through C_0 will have the effect of partially resetting the first stage compression and the step-up transformer. The reset of the other stages and the induction cells will be done by a separate pulse generator just prior to initiating the pulse sequence. The optimum saturable reactor is obtained by designing a time compression of about 3:1 and with three stages the total compression will be about 27:1. The thyratron switch will discharge C_0 in about 6.8 μs. As the magnetic switch, $S1$, saturates, it will discharge C_1 into the transformer primary with a time period of 2.25 μs. This primary voltage of 30 kV will be stepped up to 428 kV and charge C_2 with a $l - \cos(\omega t)$ waveform. The magnetic switch S_2 is designed to saturate at the peak of this waveform, which will charge the pulse forming network in 750 ns. Finally, the saturable reactor S_3 switch the PFN energy at the peak of that waveform, delivering the energy to the seven cells. The desired waveform will be achieved by tailoring the temporal impedance of the PFN to that of the nonlinear load of the cells. Further waveform tailoring is done with series inductors and an RC compensation network in the boxes on each side of the cells.

The total energy that must be switched by the thyratrons includes the system losses, and amounts to 2.5 kJ. This energy is stored in capacitor $C_0 = 5.66$ μF and is switched into C_1 through inductor $L_1 = 0.828$ μH with a series impedance $Z_0 = 0.382$ Ω, resulting

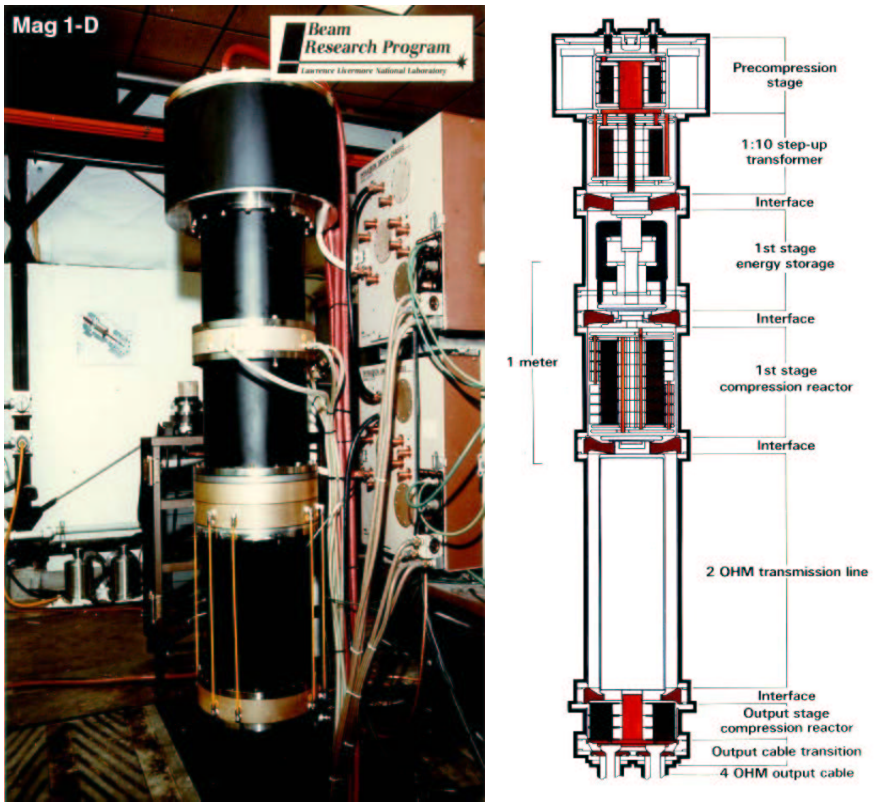

Figure 9.12: 500 J Mag 1-D magnetic pulse compression modulator driving the ETA II accelerator.

in a peak half-sine-wave current of 28 kA, for a peak power of 2.3 GW. Several thyratron options are available. The highest continuous-power thyratrons are the ceramic-envelope units, while the glass-envelope units are capable of nearly as high a peak power with low average power capability. Since the average power is moderate (38 kW) the appropriate choice for technical and economic reasons is the glass- envelope unit. To carry the 78 kA peak current, twelve parallel devices are used. To insure current sharing, each thyratron will switch its own capacitor which is $C_0/12 = 0.47$ μF. Except for thyratron replacement every 20,000 hours or more of operation, the pulse compression systems should be maintenance free since all components are passive devices.

9.1.6.3 IL2 pulse compressor

The pulse for the IL2 accelerator has a duration (FWHM) of 100 ns. Assuming an additional 5% loss (since the pulse compression system has to go one step further), the total input energy for seven cells would be $U = 1.6$ kJ and, at 15 Hz, would result in a power requirement of 24 kW. The total power requirement for IL1 is 1.9 MW, and its pulse duration is 100 ns FWHM. The shorter pulse duration would dictate an additional stage of pulse compression on the system described for IL1. However, since the energy for IL2 is 68% of IL1, it is possible to achieve the shorter pulse duration with the same number of stages simply by initiating the compression process with a shorter pulse. The design of each stage, of course, will be different and the transformer will have a step-up of 12:1. For IL2, $C_0 = 3.78$ μF and the compression for three stages is 36 for an initial discharge time of 3.6 μs with $L_0 = 0.347$ μH and $Z_0 = 0.303\Omega$. The peak current required of the twelve thyratrons is 99 kA, or 8.25 kA each.

9.1.6.4 IL3 pulse compressor

The pulse duration for IL3 is 380 ns FWHM. A pulse compression similar to IL1 with three stages is used. The transformer will have a step-up of about 10:1, and the three saturable reactors will be similar to those in IL1. The energy at the input is $U = 2$ kJ and, at 15 Hz average repetition rate, the input power per seven cells is 29.3 kW and the total imput power is $P_t = 2.34$ MW. With the input energy of 2 kJ, the capacitor $C_0 = 4.34$ μF and with an initial discharge time $t_0 = 10.3\mu$s, the inductor $L_0 = 2.46$ μH, and the series impedance $Z_0 = 0.753\Omega$, which results in a peak current of 40 kA. The total power required for IL1, IL2 and IL3 at 15 Hz average repetition rate is 8.2 MW. Including the efficiency of 90% for the DC charging power supplies, the total 60-Hz power requirement (see Table. 9.2) will be very nearly 9 MW.

Table 9.2: Energy and power requirements. * Assuming 90% efficiency.

Unit	Length (m)	Pulser energy (J/m)	Total energy (kJ)	P_{total} (15 Hz)* (kW)
IL1	100	2548	254.8	4247
IL2	80	1590	126.9	2115
IL3	80	1951	156.1	2602
Total power required from grid				8964

9.1.7 Mechanical Systems

In order to achieve the desired gradient for the three induction linacs, the induction cells are driven by the pulsing system in units of seven. Hence, these cells are mechanically assembled into one module by bolting together seven cells.

The individual cores would be assembled at the plant. The mandrel on which the amorphous material is wound supports the complete core. An additional support cradle is included on the OD of the core to insure that there is no sagging (Fig. 9.13). As specified under electrical requirements, the cores are wound with 101.6 mm wide ribbon with 3 μm mylar between layers and protruding 3 mm beyond the ribbon. As assumed earlier in this section, the complete core has a packing factor (PF) of about 75%.

The high-voltage insulator, which is the oil-to-vacuum interface, is assembled in seven sections for each module and voltage grading of each section is provided by making contact with the appropriate cell. Each section has a gradient ring, which insures that the field lines enter the insulator at an angle of about 30° to provide maximum voltage holding (Fig. 9.6). The seven section insulator is made of "Mykroy/Mycalex" and will be glued together as in the DARHT accelerator (Fig. 9.14). The induction module housing is fabricated and assembled using seven large rings fastened together by outside fixtures similar to those used in the Relativistic Two-beam Accelerator (RTA) at LBNL. The whole module is supported on the OD from these rings by a six-strut support system (Fig. 9.15). The support system allows for excellent alignment of each module with respect adjacent modules and the absolute beam line.

The vacuum system will consist of turbo pumps and cryopumps located every 5-10 modules. These pumps will be connected to a roughing line alongside the accelerator. Beam position and total current diagnostics will also be located at the pump-out station. Each module with its downstream SC solenoid magnet is assembled and aligned prior to installation in the beamline. After installation in the beamline, the module is aligned and the vacuum seal is fastened.

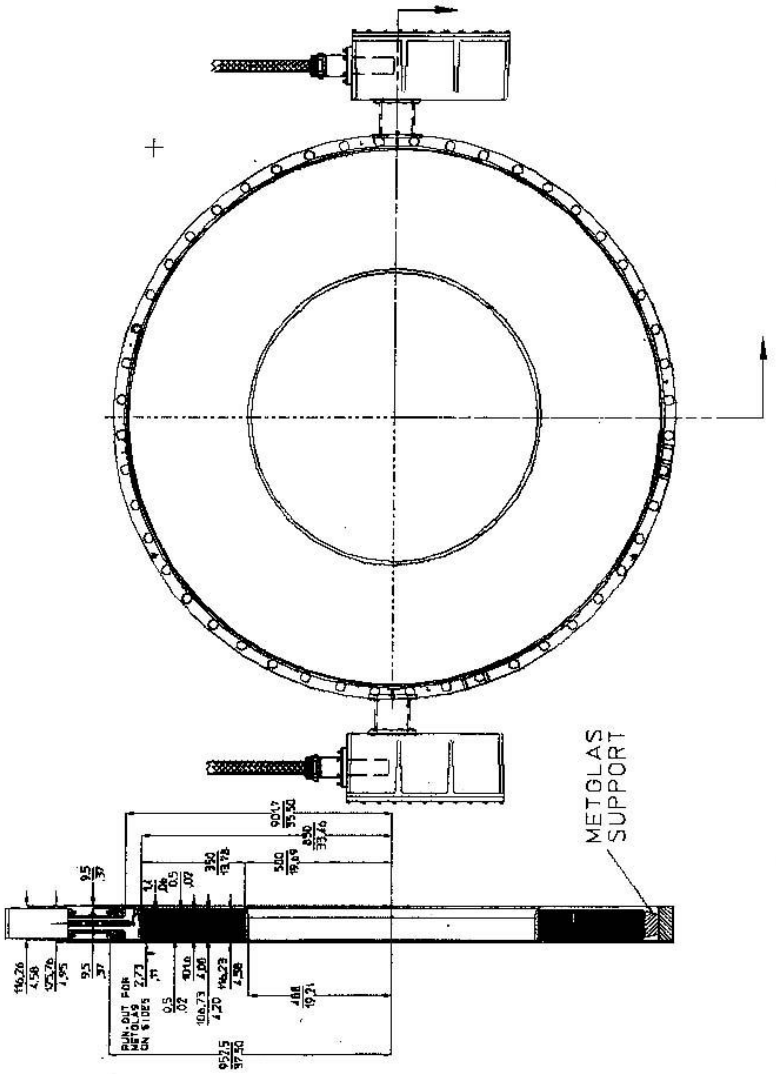

Figure 9.13: Metglas single-cell assembly.

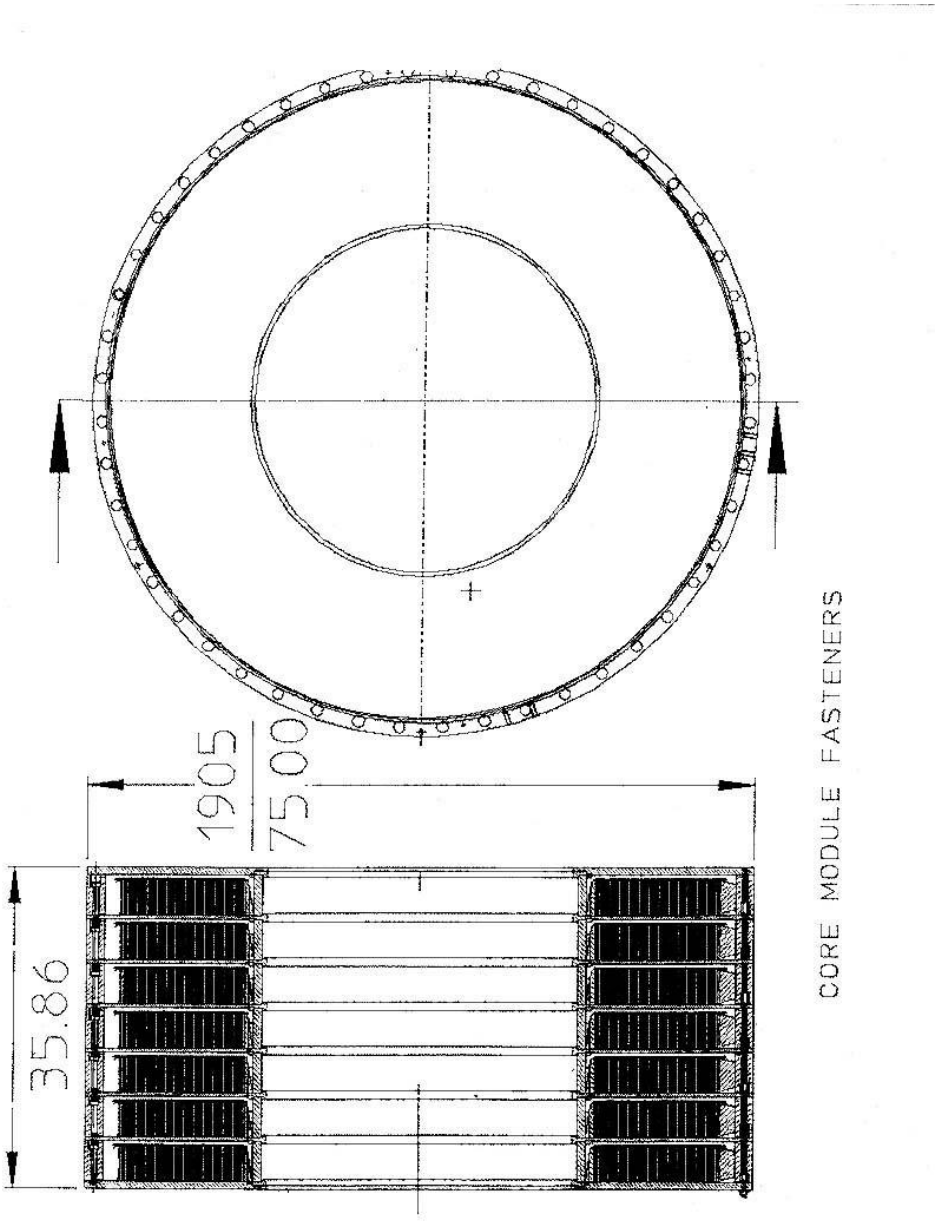

Figure 9.14: Seven-cell housing that forms one accelerator module.

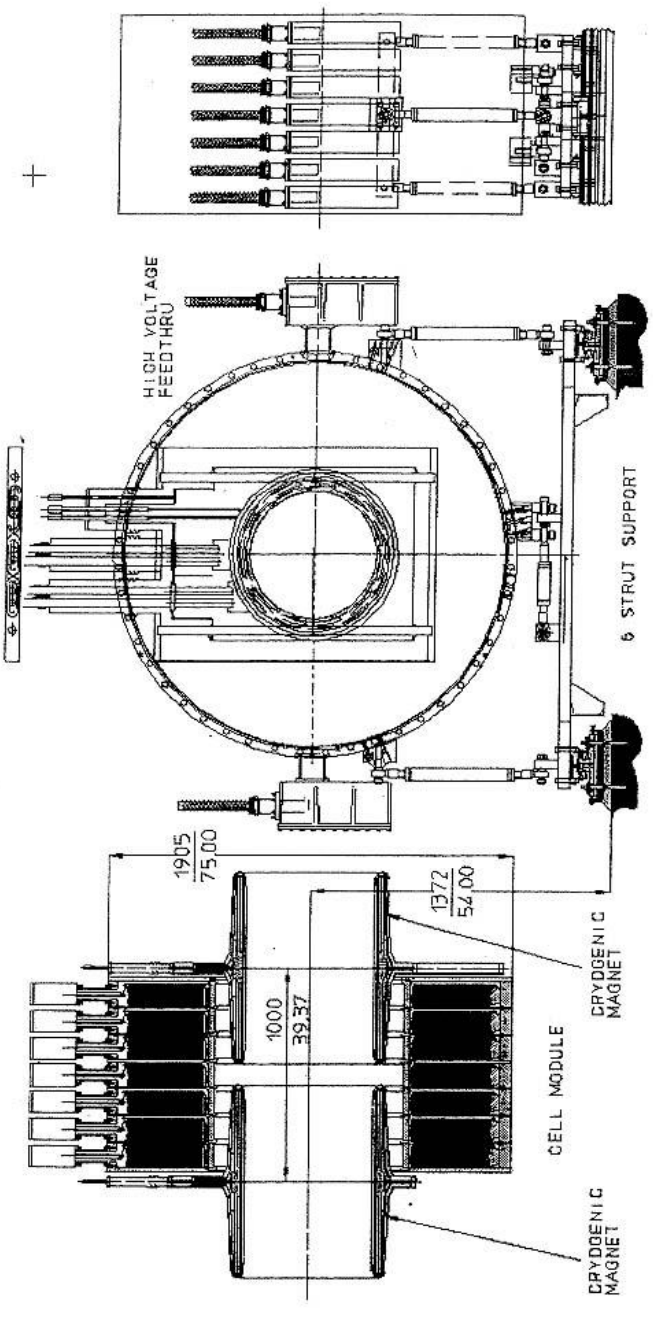

Figure 9.15: Six-strut module support system.

Bibliography

[1] N.C. Christofilos, *High-Current Linear Induction Accelerator for Electrons*, Rev. Sci. Instrum., **35**, July (1964).

[2] N. Holtkamp and D. Finley, eds., *A Feasibility Study of a Neutrino Source Based on a Muon Storage Ring*, Fermilab-Pub-00/108-E (2000), Chapter 5, p. 5-4. http://www.fnal.gov/projects/muon_collider/nu-factory/nu-factory.html

[3] M.J. Burns, et al., *DARHT Accelerators Update and Plans for Initial Operation*, Proc. 1999 Acc. Conf., p.617.

[4] W.S. Melville, *The Use of Saturable Reactors as Discharge Devices for Pulse Generators*, Institute of Electrical Engineers, **98**-Part III, May (1951).

[5] D.L Birx, *An Investigation into the Repetition Rate Limitations of Magnetic Switches*, UCRL-87278, (1982), Lawrence Livermore National Laboratory.